Check for updates

The substitution of a single amino acid with its enantiomer for control over the adjuvant activity of self-assembling peptides†

Mingyu Li,‡[a] Mingyuan Liu,‡[c] Yuna Shang,[d] Chunhua Ren, [ID] *[b] Jianfeng Liu,[b] Hongxing Jin*[a] and Zhongyan Wang [ID] *[b]

The substitution of a single amino acid with its enantiomer may lead to variations in self-assembled nanostructures and biological functions. In this study, we reported three novel heterochiral peptide hydrogels, Nap-G^DFFY (gel-1), Nap-GF^DFY (gel-2) and Nap-GFF^DY (gel-3), from Nap-GFFY via the substitution of a single amino acid with its enantiomer. We found that the resulting hydrogels possessed diverse self-assembly behaviors and adjuvant activities. Compared to the homochiral L-gel formed from Nap-GFFY, gel-1 was basically similar, gel-2 exhibited a medium improvement in immunocompetence tuning ability, and gel-3 showed the better self-assembly of nanofibers with superior mechanical properties and the ability for slow antigen release. Moreover, the adjuvant effect of gel-3 was prominent, promoting both specific antibody titers and the production of cytokines. Besides, this regulation was more remarkable with respect to enhancing cellular immune responses. Hence, we came to the conclusion in this study that the substitution of a single amino acid with its enantiomer further away from rather than closer to the end-capping group could be important and effective for biofunction regulation. Our study provides a useful strategy for tuning the properties of self-assembling peptides for different biological applications.

1. Introduction

Nanomaterials can be reasonably designed to afford corresponding biofunctions in different biological environments.[1–4] Among these, peptide-based supramolecular hydrogels have attracted extensive research interest over the last few decades because of their inherent advantages, such as their ease of design, good biocompatibility, and biodegradability.[5] More and more smart supramolecular hydrogels have been developed, and they have shown excellent results in nanomedicine,[6–9] tissue engineering,[10,11] vaccine adjuvants,[12–14] and disease detection.[15–17] The self-assembly properties of peptides are sequence-dependent[18,19] and they are also influenced by further fine-tuning of the chemical structure;[20–24] this leads to further variations of self-assembled nanostructures and biofunctions. Fine-tuning the chemical structure of a peptide, especially substituting a single amino acid for its enantiomer, to control its self-assembly behavior is sometimes difficult to understand, but there is evidence that it makes a lot of sense.[25–27]

D-Peptide-based nanomaterials that exhibit better biological functionality than their enantiomer L-peptides have been widely reported. Xu et al. developed a series of D-peptide hydrogels formed via enzyme-instructed self-assembly (EISA) that can selectively kill cancer cells.[28,29] D-Amino acids covalently conjugated with nonsteroidal anti-inflammatory drugs (NSAIDs) also have been used to boost the selectivity for inhibiting cyclo-oxygenase-2.[30] Homochiral L-peptides and D-peptides usually have similar self-assembly behaviors but distinct biological functions. D-Peptides possess higher biostability because of their inherent resistance to endogenous proteases, increasing their internal retention times. Combining L- and D-amino acids is a unique approach for constructing functional hydrogels.[31,32] Marchesan et al. developed plenty of heterochiral hydrogelators and revealed the effects of chirality on peptide self-assembly.[33,34] Heterochiral assemblies have potential applications when it comes to unprotected short peptides, with the idea that the substitution of a single amino acid with its enantiomer can result in an assembly with a different bioregulatory capacity. However, this is unclear in relation to end-capping peptide self-assemblies and their biofunctions.

[a]School of Chemical Engineering and Technology, Hebei University of Technology, Tianjin 300130, P. R. China

[b]Tianjin Key Laboratory of Radiation Medicine and Molecular Nuclear Medicine, Institute of Radiation Medicine, Chinese Academy of Medical Sciences, Peking Union Medical College, Tianjin 300192, P. R. China. E-mail: wangzhongyan@irm-cams.ac.cn

[c]College of Pharmacy, Taizhou Polytechnic College, Taizhou 225300, Jiangsu, P. R. China

[d]College of Life Sciences, Nankai University, Tianjin 300071, P. R. China

† Electronic supplementary information (ESI) available: The characterization of compounds, and rheology and cytotoxicity experiments. See DOI: 10.1039/c9ra10325b

‡ The authors equally contributed to the work.

Short peptides are usually protected by aromatic capping-groups (fluorenyl, naphthyl, *etc.*), which not only contribute to molecular self-assemblies through aromatic–aromatic interactions but also perform additional defined functions.[35,36] Naphthyl (Nap) is an excellent building block for assisting self-assembly and constructing immune adjuvants. Yang *et al.* developed two homochiral tetrapeptide hydrogels, an L-gel from Nap-GFFY and a D-gel from Nap-G^{D}F^{D}F^{D}Y, and found that the D-gel possessed better stability and vaccine adjuvant potency than its enantiomer in terms of both humoral immunity and anti-tumor cellular immunity.[37] As well as tuning the surface properties of a peptide,[38] the adjuvant activity of a self-assembling peptide is probably different after the substitution of a single amino acid with its enantiomer. Therefore, heterochirality should also be considered to regulate the adjuvant activity of aromatic-capping peptides, which could be helpful for the development of new-style vaccine adjuvants and the optimization of dosage approaches. Herein, based on Nap-GFFY, we synthesized three heterochiral peptides containing single D-amino acids and explored their self-assembly behaviors and abilities to regulate and control immunocompetence.

2. Experimental

2.1 Materials

2-Cl-trityl chloride resin was obtained from Nankai Resin Co., Ltd. L- and D-Fmoc-amino acids and *O*-benzotriazole-*N,N,N',N'*-tetramethyl-uronium-hexafluorophosphate (HBTU) were obtained from GL Biochem (Shanghai). 2-Naphthylacetic acid was obtained from Aladdin. Chemical reagents and solvents were used as received from commercial sources. Dulbecco's modified Eagle's medium (DMEM), fetal bovine serum (FBS) and penicillin/streptomycin were purchased from Gibco Corporation. EndoFit ovalbumin (OVA) (endotoxins <1 EU mg^{-1}) was purchased from InvivoGen (CA, USA). Horseradish peroxidase-conjugated goat anti-mouse IgG, IgG1, IgG2a and IgG2b were obtained from Southern Biotechnologies (AL, USA). Mouse IL-4/IFN-γ ELISA kits were purchased from Biolegend. Six-week-old female C57BL/6 mice were purchased from Beijing Vital River Laboratory Animal Technology Co., Ltd.

2.2 General methods

^{1}H NMR (Bruker ARX 400) and LC-MS (Shimadzu, 2020) methods were used to characterize the synthesized compounds. HPLC was conducted with a LUMTECH HPLC (Germany) system using a C$_{18}$ RP column with MeOH (0.05% TFA) and water (0.05% TFA) as eluents. TEM images were obtained using a HT7700 Exalens system (Hitachi, Japan). Rheology studies were performed with an AR 1500ex (TA instrument) system using a parallel plate (25 mm) with a gap of 500 μm.

2.3 Peptide synthesis

All peptides were synthesized using 2-chlorotrityl chloride resin and the corresponding *N*-Fmoc protected amino acids, with the side chains properly protected, *via* solid phase peptide synthesis (SPPS) methods. The first amino acid was loaded onto the resin

at the C-terminal with a loading efficiency of about 1.2 mmol g^{-1} 20% piperidine in anhydrous *N,N*-dimethylformamide (DMF) was used to remove the Fmoc group. Then the Fmoc-protected amino acid was coupled to the free amino group using HBTU as the coupling reagent. The growth of the peptide chain took place according to the established Fmoc SPPS protocol. After the last coupling step, excess reagents were removed by washing five times with DMF, followed by washing five times with DCM. The peptide was cleaved from the resin using 95% trifluoroacetic acid. Iced ethyl ether was then added to the concentrated solution to precipitate the crude product.

2.4 Preparation of hydrogels

5 mg of peptide was evenly scattered into 1 mL of PBS buffer solution. 1 eq. of Na$_2$CO$_3$ was used to neutralize the carboxylic acids of the peptide and set the final pH value at 7.4. Then, the peptide suspension was heated using an alcohol lamp until it completely dissolved at about 80 °C. A gel formed after cooling to room temperature.

2.5 Transmission electron microscopy

A negative staining technique was used to observe the nano-structures of the hydrogels. 15 μL of hydrogel sample was firstly loaded onto a carbon-coated copper grid for 2 minutes, which was then rinsed with water twice. Subsequently, the sample was stained with 1% uranyl acetate for 1 minute. Finally, the grid was placed in a desiccator for 6 h before observation.

2.6 Circular dichroism spectroscopy

Circular dichroism (CD) spectra were obtained using a BioLogic (MOS-450) system. Hydrogel samples were placed in a 0.1 cm quartz spectrophotometer cell (20-C/Q/0.1). The wavelength range was from 190 to 280 nm. The acquisition period was 0.5 s and the step size was 0.5 nm. The resultant CD spectrum was acquired after subtracting the solvent background.

2.7 Thioflavin T binding assay

1 mL samples of different concentrations were prepared and placed in a microwell plate. Subsequently, 20 μL of thioflavin T (ThT) solution (20 μM) was added on top of the samples. After incubation for 20 minutes, ThT fluorescence was determined at an excitation wavelength of 440 nm using a spectrofluorophotometer. The fluorescence intensity of a sample was obtained on the basis of the peak value of emission at about 484 nm.

2.8 Rheology

Rheology tests were done using an AR 1500ex (TA instrument) system; a 25 mm parallel plate was used during the experiments with a gap of 500 μm. For the dynamic frequency sweep measurements, samples were directly transferred to the rheometer and tested from 1–100 rad s^{-1} at a strain of 1%. Finally, a dynamic strain sweep at a frequency of 1 rad s^{-1} was conducted. All samples were tested at a temperature of 37 °C.

2.9 Preparation of OVA-RhB and antigen release assays *in vitro*

To obtain rhodamine-B-modified OVA (OVA-RhB), 5 mg of OVA was dissolved in 1 mL of PBS and 2 eq. of rhodamine B isothiocyanate (J & K scientific) was then added. 1 eq. of Na_2CO_3 was added to adjust the final pH to 7.4. The mixture was put into a dialysis bag (interception molecular weight: 1000 Da) and stirred at 4 °C for 24 h. The protein concentration after dialysis was determined using a NanoDrop analyzer. The *in vitro* release profiles of OVA-RhB in hydrogels were studied at 37 °C. 150 μL of hydrogel (0.5 wt%) containing 75 μg of OVA-RhB was used for the measurements. 150 μL of PBS solution (pH = 7.4) was added on top of the gel; 100 μL of solution was taken out at the desired time point and 100 μL of fresh PBS solution was added back in. The absorbance value of OVA-RhB was determined at 560 nm using a microplate reader (Thermo Scientific Varioskan Flash) to calculate the release percentage of OVA-RhB from the gel.

2.10 Hydrogel vaccine formulation

All hydrogel vaccines were prepared using endotoxin-free PBS buffer (pH = 7.4) at a final concentration of 0.5 wt%. 25 μL of endotoxin-free OVA stock solution (20 mg mL^{-1}) was added and mixed with 975 μL of hydrogel. Then, OVA was dispersed evenly in the hydrogel under vortex and the mixture was stabilized at room temperature for half an hour. The final concentration of OVA in the hydrogel was 500 μg mL^{-1}.

2.11 Vaccination

The hydrogel vaccines were first shaken into a viscous liquid before immunization. Female C57BL/6 mice were randomly distributed, and each group contained 5 mice. Mice were treated *via* subcutaneous injection with 100 μL of a specific vaccine (0.5 wt% hydrogel including 50 μg of OVA vaccine; 100 μL of PBS with 50 μg of OVA; or 50 μg of OVA with 25 eq. of alum, respectively) in the groin at day 0. Further immunization was carried out at day 14. Serum was collected after 7 days for antibody detection.

2.12 Measurements of specific antibodies

OVA-specific antibody responses in mice were examined *via* an enzyme-linked immunosorbent assay (ELISA) approach. 96-well ELISA plates were coated with 10 μg mL^{-1} OVA and stored at 4 °C overnight. After washing with PBST (PBS buffer containing 0.05% Tween 20) four times, the plates were blocked with blocking buffer (1% BSA in PBST) for 1 h at room temperature. Individual antiserum samples were serially diluted in the blocking buffer and incubated in the plates for 2 h at room temperature. After 5 washes with PBST, the plates were incubated with goat anti-mouse IgG horseradish peroxidase for 1 h. Antibody binding was assessed through adding 100 μL of 3,3′,5,5′-tetramethylbenzidine peroxidase substrate (TMB). The substrate reaction was terminated *via* adding 100 μL of 2 M H_2SO_4. The plates were immediately read at 450 nm using an ELISA reader. Antibody titers were calculated based on reciprocal serum dilution, giving O.D. values >0.1 standard deviations above a background level that was calculated using PBS at the same dilution.

2.13 Splenocyte cytokine production

After serum was extracted, the spleens from each group were taken out and ground. After erythrocyte lysis was carried out, splenocytes (5×10^6 cells per mL) were collected and seeded in 24-well plates with 1640 medium containing 10% FBS and 1% PS; subsequently, they were re-stimulated with soluble OVA (50 μg mL^{-1}) in a carbon dioxide incubator for 96 h. The production of IFN-γ and IL-4 in splenocyte culture supernatants was detected using ELISA kits (Biolegend, San Diego, CA, USA).

2.14 Cytotoxicity evaluation

The cytotoxicities of the hydrogels were evaluated *via* CCK-8 assays. RAW 264.7 cells and splenocytes separated from C57BL/6 mice were respectively cultured in 96-well plates at a density of 1×10^4 cells per well with a medium volume of 100 μL. After incubation for 24 h, the medium was removed and 100 μL of fresh medium containing a series of peptide concentrations was added. 72 h later, 10 μL of CCK-8 was added into the wells. After 4 h, the optical density of the solution at 597 nm was measured using a microplate reader (BioTek, USA), and cells without any treatment were used as the control. The percentage cell viability was calculated according to the following formula:

$$\text{Percentage cell viability (\%)} = OD_{sample}/OD_{control} \times 100\%.$$

3. Results and discussion

3.1 Peptide synthesis and hydrogel preparation

The tetrapeptide Nap-GFFY contains three amino acid sites with transformable chirality (Fig. S7†). As shown in Fig. 1, we replaced the L-amino acid with the corresponding D-amino and obtained three possible heterochiral hydrogelators: Nap-G^{D}FFY
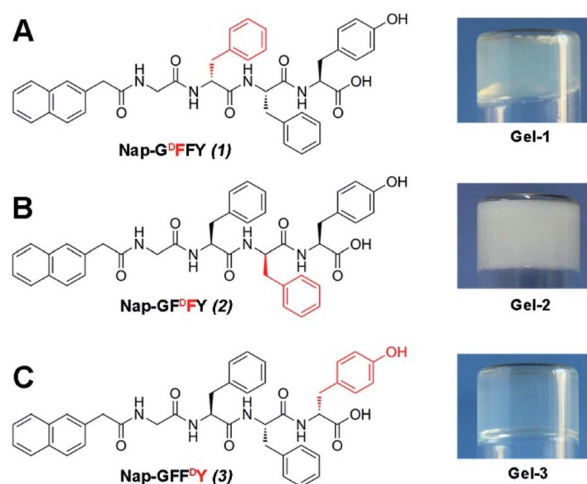

Fig. 1 The chemical structures and optical images of (A) Nap-G^{D}FFY, (B) Nap-GF^{D}FY and (C) Nap-GFF^{D}Y hydrogels.

(1), Nap-GF^{D}FY (2), and Nap-GFF^{D}Y (3). The compounds were synthesized *via* solid phase peptide synthesis (SPPS) and were depurated *via* reverse phase high performance liquid chromatography (HPLC). Homochiral Nap-GFFY can form a transparent hydrogel (L-gel) within 2 minutes after heating at a concentration of 0.5 wt% (Fig. S7, ESI†). Nap-G^{D}FFY can form semitransparent hydrogel (gel-1) in phosphate buffer saline (PBS) solution (pH = 7.4) within 10 minutes at a concentration of 0.5 wt% following a heating–cooling procedure. Under the same conditions, Nap-GF^{D}FY can form a white and opaque hydrogel (gel-2) within 30 minutes, indicating the formation of large aggregates. Nap-GFF^{D}Y can form a transparent hydrogel (gel-3) within 5 minutes. The minimum gelation concentrations (MGCs) for these hydrogels were about 0.2, 0.5, and 0.1 wt%, respectively. Compared to the homochiral L-gel, the substitution of a single amino acid with its enantiomer in the peptide sequence had a distinct effect on the self-assembling capacity and resulted in different hydrogels.

3.2 Nanostructural characterization of the hydrogels

The nanostructures of all hydrogels were then observed *via* transmission electron microscopy (TEM). The homochiral L-gel showed a nanostructure made up of fibers with a diameter of about 10 nm (Fig. 2A). However, heterochiral gel-1, gel-2, and gel-3 exhibited disparate morphologies. Gel-1 had thicker nanofibers with a diameter of about 15 nm (Fig. 2B), and gel-3 had thin nanofibers with a diameter of about 6 nm (Fig. 2D). The flexible nanofibers intertwined with each other to support hydrogelation. In particular, Nap-GF^{D}FY in gel-2 self-assembled into sheet-like structures with a width of hundreds of nanometers and a length of a few micrometers (Fig. 2C), similar to nanosheet assemblies from peptoids.[39] Apart from similar aromatic–aromatic interactions from naphthyl capping, the aromatic stacking of side chains had a critical impact on the molecular arrangement. Unlike Nap-G^{D}FFY and Nap-GFF^{D}Y, the three aromatic groups of Nap-GF^{D}FY were on the same side of the peptide backbone, probably resulting in stable aggregation.[33] The substitution of a single amino acid with its enantiomer changed the nanostructures of the hydrogels to varying degrees, indicating their biofunctional tunability.

3.3 Secondary structures of peptides

The secondary structures of the three heterochiral hydrogelators at different concentrations were measured *via* circular dichroism. As shown in Fig. 3A, 1 exhibited no signs of secondary structure at a concentration of 125 μg mL^{-1}. As the concentration increased, the spectrum showed a slight change. When the concentration was increased to 175 μg mL^{-1}, 1 showed a β-sheet structure with a negative peak at 192 nm and a positive peak at 211 nm (Fig. 3A). Similarly, 2 also exhibited a β-sheet structure, with a negative peak at 193 nm and a positive peak at 210 nm, as the concentration was increased to 200 μg mL^{-1} (Fig. 3B). In particular, 3 showed a distinct secondary structural change at a concentration of 100 μg mL; a typical β-sheet structure, on the basis of a positive peak at 197 nm followed by a negative peak at 218 nm, emerged when the concentration was increased to 125 μg mL^{-1}, effectually promoting ordered molecular arrangement and the formation of uniform nanofibers. These results were further supported by thioflavin T (ThT) binding assays. ThT emission exhibited little change when the concentrations of 1, 2 and 3 were below 175, 200 and 125 μg mL^{-1}, respectively. Hereafter, the emission intensities showed an almost linear increase with an increase in concentration, indicating that the formation of greater numbers of nanostructures with a β-sheet secondary structure was a cause of enhanced molecular assembly.

3.4 Mechanical properties of the hydrogels

The mechanical properties of these hydrogels were characterized using a rheometer at 37 °C. We first performed dynamic time sweeps and found that all hydrogels gradually reached
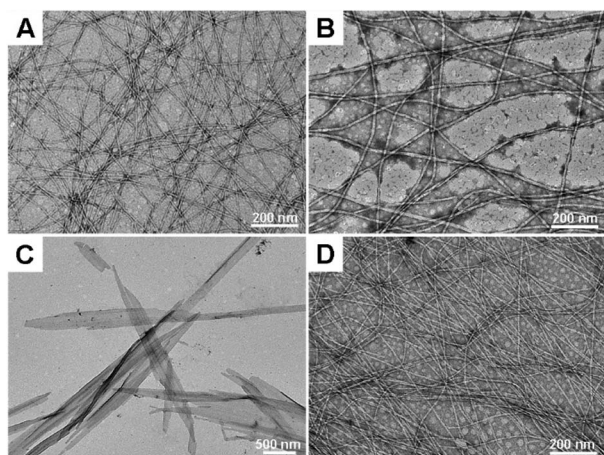

Fig. 2 The nanostructures of (A) L-gel, (B) gel-1, (C) gel-2 and (D) gel-3 at a concentration of 0.5 wt%.
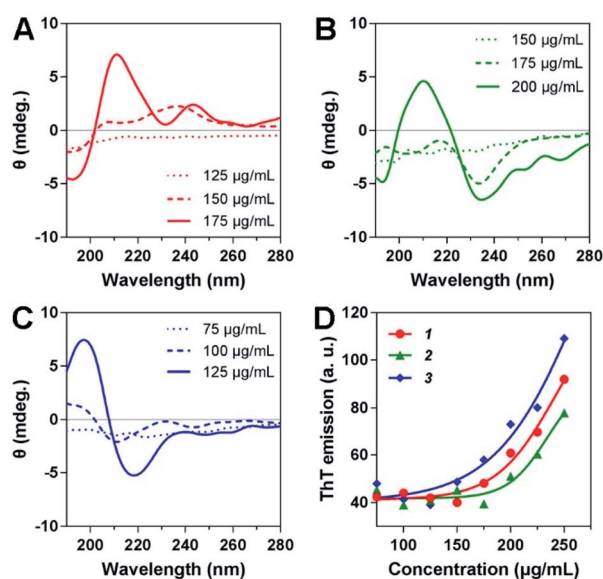

Fig. 3 Circular dichroism spectra of (A) 1, (B) 2, and (C) 3 at different concentrations. (D) ThT emission intensities in the presence of 1, 2 and 3 at elevated concentrations.
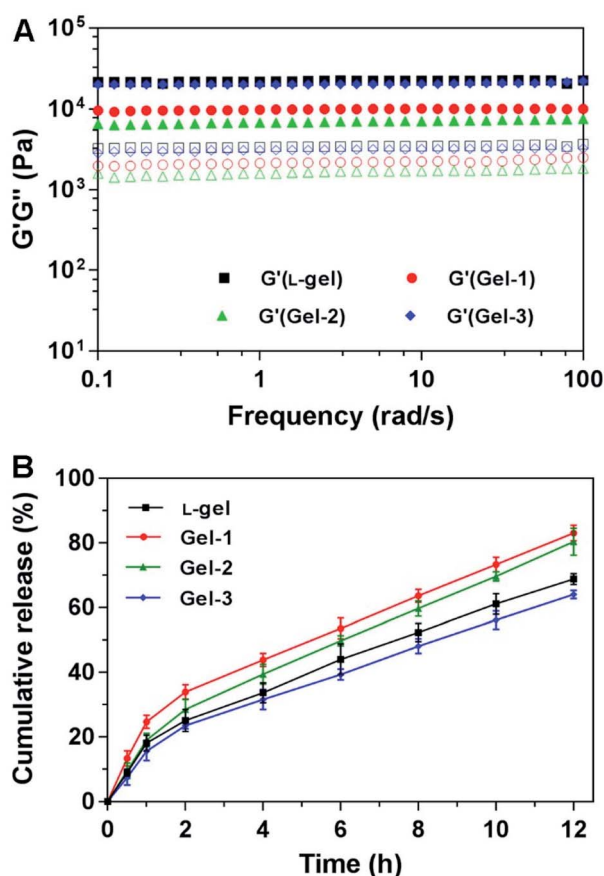
Fig. 4   (A) Dynamic frequency sweeps of L-gel, gel-1, gel-2 and gel-3 at a concentration of 0.5 wt% under a strain of 1% at 37 °C (the solid icons represent G', the corresponding hollow icons represent G''). (B) The cumulative release curve of OVA-RdB from L-gel, gel-1, gel-2 and gel-3 at a concentration of 0.5 wt% in vitro at 37 °C over 12 hours.

stability within 60 minutes, a precondition for dynamic frequency sweeps (Fig. S8A, ESI†). According to dynamic strain sweeps, the mechanical properties of the hydrogels were steady at a strain of 1%, which served as an appropriate precondition for dynamic frequency sweeps (Fig. S8B, ESI†). As shown in Fig. 4A, all gels exhibited weak frequency dependencies over the range of 0.1–100 rad s^{-1}. The elasticity (G' or storage modulus) values of the gels were about 3–10 times bigger than their corresponding viscosity (G'' or loss modulus) values. The G' value of gel-3 was more than 10^4 Pa and was close to that of L-gel. The G' value of gel-1 was close to 10^4 Pa. Gel-2 possessed a G' value of less than 10^4 Pa. The more-dense nanofiber network endowed gel-3 with better mechanical properties and resistance to external forces for controllable release. The substitution of a single amino acid with its enantiomer gave the corresponding gels different rheological properties. Moreover, these mid-range mechanical properties implied that the gels would be injectable for vaccination and other biological applications.

3.5   Antigen release *in vitro*

To evaluate the controllable release capacity of the hydrogels, the antigen release profiles from the hydrogels *in vitro* were studied

through ultraviolet absorption at 37 °C. The rhodamine B-modified antigen (OVA-RhB) was first mixed into the gels under vortex at a weight ratio of 10 : 1 (peptide : OVA) for vaccine generation. The antigen was evenly wrapped in nanofiber networks or nanosheets. During the 12 h period, antigen was gradually released from the four gels. As shown in Fig. 4B, L-gel exhibited slow release behavior, and approximately 70% of the total antigen was released within 12 h. Gel-1 and gel-2 had faster release profiles than the other gels, and 83% and 80% of the total antigen were released from the gels, respectively. However, gel-3 exhibited a slower release ratio, and only 64% of the total antigen was released over the same time period. These results were consistent with the rheological behavior, as gels with better mechanical properties had better sustained release capabilities. The hydrogels can slowly release antigen, acting as an antigen warehouse, thereby ensuring sustained stimulation of the immune system by antigen and enhancing the organism immune response.

3.6   Immunization and antibody measurements

The adjuvant efficacies of the above hydrogels were subsequently evaluated by vaccinating 6-week-old female C57BL/6 mice. At day 0, the mice were injected subcutaneously (s.c.) with different vaccines (100 μL per mouse) in the groin. OVA, aluminium hydroxide (alum), and L-gel were assigned as control groups. Secondary immunization at the same dose was performed at day 14 to boost the immune responses (Fig. 5A). After another seven days had passed, mice serum samples were obtained and the OVA-specific antibody titers were detected through an enzyme-linked immunosorbent assay (ELISA) approach.

As shown in Fig. 5B, compared to the OVA group, all the adjuvants vastly increased the expression of IgG antibodies. As an adjuvant approved by the Food and Drug Administration (FDA), alum enhanced IgG expression 106-fold compared with the OVA group. L-gel had analogous potency to the alum adjuvant. Interestingly, the gel-1, gel-2 and gel-3 groups showed different immunocompetences due to the substitution of a single amino acid with its enantiomer. They increased IgG titers 98-, 163- and 341-fold, respectively (Fig. 5B). Gel-1 showed little difference after the substitution of a single amino acid with its enantiomer, exhibiting an equivalent IgG titer value to L-gel. Gel-2 showed a 1.6-fold enhancement compared to gel-1. Nevertheless gel-3 exhibited better bioactivity than the other two heterochiral gels. For IgG subclasses, the production of IgG1, IgG2a and IgG2b in the heterochiral gel groups was also raised to different degrees, and gel-3 had a prominent effect (Fig. 5C–E). Compared to the homochiral L-gel, gel-3 promoted IgG1 2.6-fold and IgG2a 3.8-fold; gel-2 promoted IgG1 1.7-fold and IgG2a 1.6-fold. However, gel-1 basically resulted in no increase in the production of IgG1 and IgG2a. The results indicated that the substitution of a single amino acid with its enantiomer further away from the capping group had greater influence on adjuvant activity than substituting one close to the capping group.

3.7   Splenocyte cytokine analysis

To more deeply understand the adjuvant effects of different heterochiral hydrogels, we then evaluated two representative
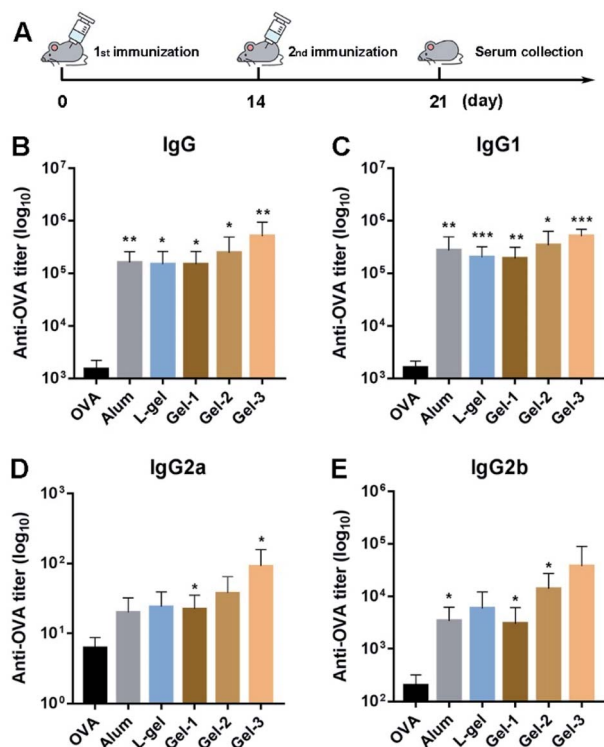
Fig. 5 (A) The program of vaccination. The production of OVA-specific (B) IgG and the subtypes (C) IgG1, (D) IgG2a and (E) IgG2b (bars show mean ± SD; differences among groups are determined using one-way analysis of variance (ANOVA) analysis; asterisks represent significant difference between the OVA group and another group; *p < 0.05, **p < 0.01, ***p < 0.001).

Fig. 6 The production of (A) IL-4 and (B) IFN-γ in splenocyte culture supernatants (bars show mean ± SD; differences among groups are determined using one-way analysis of variance (ANOVA) analysis; asterisks represent significant difference between the OVA group and another group; *p < 0.05, **p < 0.01, ***p < 0.001).

3.8 Biocompatibility of the hydrogels

Finally, we evaluated the cytotoxicities of all the gels *via* analyzing the weights of major organs from vaccinated mice, including lymph glands, hearts, livers, spleens, lungs, and kidneys. Compared to aluminium hydroxide, which is approved by the Food and Drug Administration (FDA), the gels had little effect on the organs (Fig. S9, ESI†). We also measured the cytotoxicities of the gels toward splenocyte immune cells and RAW 264.7 cells *via* CCK-8 assays *in vitro*; the results exhibited that the gels had very little inhibitory effect below a concentration of 320 μg mL^{-1} (Fig. S10, ESI†). These results demonstrated that our gels possessed good biocompatibility and were suitable for biomedical applications.

4. Conclusions

Fine-tuning the chemical structures of self-assembling peptides may lead to variations in self-assembled nanostructures and changes in biological function. Combining L- and D-amino acids is a unique approach for constructing functional hydrogels. In this study, we synthesized three heterochiral peptides with aromatic end-capping groups and explored their self-assembly abilities and adjuvant activities. Under the same conditions, the three peptides formed different hydrogels and exhibited dissimilar nanostructures. In particular, gel-3 exhibited better self-assembly abilities, with superior mechanical properties and slow release abilities. The gels also promoted specific immune responses to different degrees. Compared with the homochiral L-gel, the heterochiral gel-1 was basically useless for immune activation, while gel-2 exhibited medium regulation. However, the adjuvant effect of the heterochiral gel-3 was dominant in relation to promoting specific antibody titers and the production of cytokines. Conclusively, in this study, the substitution of a single amino acid with its enantiomer further away from the end-capping group could be more important and effective for tuning biofunctionality than substitution close to the end-capping group. Our study provides a useful strategy for tuning the biofunctionality of self-assembling peptides, contributing to the development of novel biomaterials for different biological applications.

cytokines: IL-4 and IFN-γ. The spleens from immunized mice were isolated into single-cell suspensions and the re-stimulation of OVA antigens was carried out. After 4 days of culturing, the splenocyte supernatants were collected for ELISA measurements. As shown in Fig. 6, the production of IL-4 and IFN-γ was greatly increased in all hydrogel vaccine groups. Compared to the homochiral L-gel, heterochiral gel-1 and gel-2 had slight advantages in promoting IL-4 (1.1-fold), and gel-3 showed better performance (1.3-fold) than the other gels (Fig. 6A). As an important Th2 cytokine, IL-4 acts on B cell maturation and promotes the production of IgG1 antibodies, suggesting that the heterochiral gels had the ability to regulate humoral immune responses, and gel-3 was the best of the heterochiral gels. However, this adjuvant activity was more evident when examining Th1 immune responses. Compared to L-gel, gel-1, gel-2 and gel-3 enhanced IFN-γ 1.1-, 1.7- and 2.3-fold, respectively (Fig. 6B), which were greater improvements than in the case of IL-4 regulation. IFN-γ secreted by Th1 cells can ultimately induce IgG2a expression by B cells, in keeping with the above results relating to IgG2a titers. The substitution of a single amino acid with its enantiomer promoted a hierarchical regulating effect on humoral and cellular immune responses, and the chirality of the amino acid close to the end-capping group was important for immunoregulation.
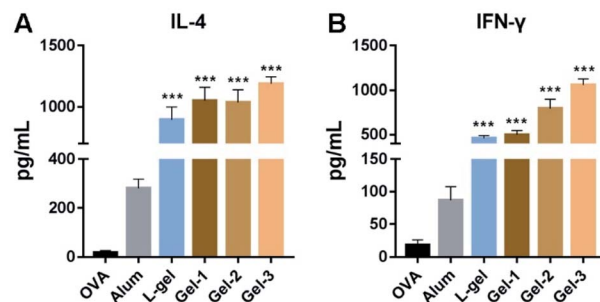
Ethical statement

Conflicts of interest

There are no conflicts to declare.

Acknowledgements

References

1 J. Yao, M. Yang and Y. Duan, *Chem. Rev.*, 2014, **114**, 6130–6178.
2 B. Pelaz, P. del Pino, P. Maffre, R. Hartmann, M. Gallego, S. Rivera-Fernandez, J. M. de la Fuente, G. U. Nienhaus and W. J. Parak, *ACS Nano*, 2015, **9**, 6996–7008.
3 F. Pu, J. Ren and X. Qu, *Chem. Soc. Rev.*, 2018, **47**, 1285–1306.
4 X. Zheng, H. Mao, D. Huo, W. Wu, B. Liu and X. Jiang, *Nat. Biomed. Eng.*, 2017, **1**, 0057.
5 X. Du, J. Zhou, J. Shi and B. Xu, *Chem. Rev.*, 2015, **115**, 13165–13307.
6 H. Shigemitsu, T. Fujisaku, W. Tanaka, R. Kubota, S. Minami, K. Urayama and I. Hamachi, *Nat. Nanotechnol.*, 2018, **13**, 165–172.
7 H. Wang, Z. Feng, Y. Qin, J. Wang and B. Xu, *Angew. Chem., Int. Ed.*, 2018, **57**, 4931–4935.
8 J. Wu, Z. Zheng, Y. Chong, X. Li, L. Pu, Q. Tang, L. Yang, X. Wang, F. Wang and G. Liang, *Adv. Mater.*, 2018, **30**, 1805018.
9 Y. Shang, Z. Wang, R. Zhang, X. Li, S. Zhang, J. Gao, X. Li and Z. Yang, *Chem. Commun.*, 2019, **55**, 5123–5126.
10 Y. Shang, D. Zhi, G. Feng, Z. Wang, D. Mao, S. Guo, R. Liu, L. Liu, S. Zhang, S. Sun, K. Wang, D. Kong, J. Gao and Z. Yang, *Nano Lett.*, 2019, **19**, 1560–1569.
11 D. J. Smith, G. A. Brat, S. H. Medina, D. Tong, Y. Huang, J. Grahammer, G. J. Furtmüller, B. C. Oh, K. J. Nagy-Smith, P. Walczak, G. Brandacher and J. P. Schneider, *Nat. Nanotechnol.*, 2016, **11**, 95–102.
12 J. S. Rudra, Y. F. Tian, J. P. Jung and J. H. Collier, *Proc. Natl. Acad. Sci. U. S. A.*, 2010, **107**, 622–627.
13 Z. Wang, C. Liang, F. Shi, T. He, C. Gong, L. Wang and Z. Yang, *Nanoscale*, 2017, **9**, 14058–14064.
14 Z. Wang, Y. Shang, Z. Tan, X. Li, G. Li, C. Ren, F. Wang, Z. Yang and J. Liu, *Theranostics*, 2020, **10**, 657–670.
15 P. Zhang, Y. Cui, C. F. Anderson, C. Zhang, Y. Li, R. Wang and H. Cui, *Chem. Soc. Rev.*, 2018, **47**, 3490–3529.
16 C. Ren, Z. Wang, Q. Wang, C. Yang and J. Liu, *Small Methods*, 2019, 1900403.
17 C. Yang, C. Ren, J. Zhou, J. Liu, Y. Zhang, F. Huang, D. Ding, B. Xu and J. Liu, *Angew. Chem., Int. Ed.*, 2017, **56**, 2356–2360.
18 A. Lampel, S. A. McPhee, H. A. Park, G. G. Scott, S. Humagain, D. R. Hekstra, B. Yoo, P. W. Frederix, R. R. Abzalimov, S. G. Greenbaum, T. Tuttle, C. Hu, C. J. Bettinger and R. V. Ulijn, *Science*, 2017, **356**, 1064–1068.
19 Y. Shang, Y. Liao, Z. Ye, Z. Wang, L. Xiao, J. Gao, Q. Wang and Z. Yang, *Sci. China Mater.*, 2019, **62**, 1341–1349.
20 C. Yuan, W. Ji, R. Xing, J. Li, E. Gazit and X. Yan, *Nat. Rev. Chem.*, 2019, **3**, 567–588.
21 S. Mondal, G. Jacoby, M. R. Sawaya, Z. A. Arnon, L. Adler-Abramovich, P. Rehak, L. Vuković, L. J. Shimon, P. Král, R. Beck and E. Gazit, *J. Am. Chem. Soc.*, 2018, **141**, 363–369.
22 J. Wang, K. Liu, R. Xing and X. Yan, *Chem. Soc. Rev.*, 2016, **45**, 5589–5604.
23 Z. Wang, C. Liang, Y. Shang, S. He, L. Wang and Z. Yang, *Chem. Commun.*, 2018, **54**, 2751–2754.
24 C. Yang, X. Ren, D. Ding, L. Wang and Z. Yang, *Nanoscale*, 2016, **8**, 10768–10773.
25 M. Liu, L. Zhang and T. Wang, *Chem. Rev.*, 2015, **115**, 7304–7397.
26 B. Dai, D. Li, W. Xi, F. Luo, X. Zhang, M. Zou, M. Cao, J. Hu, W. Wang, G. Wei, Y. Zhang and C. Liu, *Proc. Natl. Acad. Sci. U. S. A.*, 2015, **112**, 2996–3001.
27 K. Hu, Y. Jiang, W. Xiong, H. Li, P. Y. Zhang, F. Yin, Q. Zhang, H. Geng, F. Jiang and Z. Li, *Sci. Adv.*, 2018, **4**, eaar5907.
28 J. Li, Y. Gao, Y. Kuang, J. Shi, X. Du, J. Zhou, H. Wang, Z. Yang and B. Xu, *J. Am. Chem. Soc.*, 2013, **135**, 9907–9914.
29 J. Zhou, X. Du, N. Yamagata and B. Xu, *J. Am. Chem. Soc.*, 2016, **138**, 3813–3823.
30 J. Li, Y. Kuang, Y. Gao, X. Du, J. Shi and B. Xu, *J. Am. Chem. Soc.*, 2012, **135**, 542–545.
31 S. Marchesan, C. D. Easton, F. Kushkaki, L. Waddington and P. G. Hartley, *Chem. Commun.*, 2012, **48**, 2195–2197.
32 M. Jeena, K. Jeong, E. M. Go, Y. Cho, S. Lee, S. Jin, S. W. Hwang, J. H. Jang, C. S. Kang, W. Y. Bang, E. Lee, S. K. Kwak, S. Kim and J. H. Ryu, *ACS Nano*, 2019, **13**, 11022–11033.
33 A. M. Garcia, D. Iglesias, E. Parisi, K. E. Styan, L. J. Waddington, C. Deganutti, R. De Zorzi, M. Grassi, M. Melchionna, A. V. Vargiu and S. Marchesan, *Chem*, 2018, **4**, 1862–1876.
34 S. Marchesan, C. D. Easton, K. E. Styan, L. Waddington, F. Kushkaki, L. Goodall, K. M. McLean, J. S. Forsythe and P. G. Hartley, *Nanoscale*, 2014, **6**, 5172–5180.
35 Z. Yang, G. Liang and B. Xu, *Chem. Commun.*, 2006, 738–740.
36 C. Ou, J. Zhang, X. Zhang, Z. Yang and M. Chen, *Chem. Commun.*, 2013, **49**, 1853–1855.
37 Z. Luo, Q. Wu, C. Yang, H. Wang, T. He, Y. Wang, Z. Wang, H. Chen, X. Li, C. Gong and Z. Yang, *Adv. Mater.*, 2017, **29**, 1601776.
38 Y. Wen, A. Waltman, H. Han and J. H. Collier, *ACS Nano*, 2016, **10**, 9274–9286.
39 Z. Wu, M. Tan, X. Chen, Z. Yang and L. Wang, *Nanoscale*, 2012, **4**, 3644–3646.